Antiproton slowing down, capture, and decay in low-pressure helium gas

A. Bianconi,[1] M. Corradini,[1] A. Donzella,[1] M. Leali,[1] E. Lodi Rizzini,[1] L. Venturelli,[1] N. Zurlo,[1] M. Bargiotti,[2] A. Bertin,[2] M. Bruschi,[2] M. Capponi,[2] S. De Castro,[2] L. Fabbri,[2] P. Faccioli,[2] B. Giacobbe,[2] F. Grimaldi,[2] I. Massa,[2] M. Piccinini,[2] N. Semprini Cesari,[2] R. Spighi,[2] S. Vecchi,[2] M. Villa,[2] A. Vitale,[2] A. Zoccoli,[2] O. E. Gorchakov,[3] G. B. Pontecorvo,[3] A. M. Rozhdestvensky,[3] V. I. Tretyak,[3] M. Poli,[4] C. Guaraldo,[5] C. Petrascu,[5] F. Balestra,[6] M. P. Bussa,[6] L. Busso,[6] O. Y. Denisov,[6] L. Ferrero,[6] R. Garfagnini,[6] A. Grasso,[6] A. Maggiora,[6] G. Piragino,[6] F. Tosello,[6] G. Zosi,[6] G. Margagliotti,[7] L. Santi,[7] and S. Tessaro[7]

[1]*Dipartimento di Chimica e Fisica per l'Ingegneria e per i Materiali, Università di Brescia, Brescia and INFN, Gruppo di Brescia, Brescia, Italy*

[2]*Dipartimento di Fisica, Università di Bologna and INFN, Sezione di Bologna, Bologna, Italy*

[3]*Joint Institute for Nuclear Research, Dubna, Moscow, Russia*

[4]*Dipartimento di Energetica "S. Stecco," Università di Firenze, Firenze, Italy*

[5]*Laboratori Nazionali di Frascati dell'INFN, Frascati, Italy*

[6]*Dipartimento di Fisica Generale "A. Avogadro," Università di Torino and INFN, Sezione di Torino, Torino, Italy*

[7]*Istituto di Fisica, Università di Trieste and INFN, Sezione di Trieste, Trieste, Italy*

(Received 17 February 2004; published 7 September 2004)

Data on $\bar{p}$ slowing down and capture in helium at 1 and 0.2 mb at room temperature are presented and compared to the corresponding previously publicated data in molecular hydrogen and deuterium. A Monte Carlo simulation containing a low-energy extrapolation of measured $\bar{p}$ electronic stopping power in helium gas, screened Rutherford collisions, and simple cascade mechanisms is able to reproduce the gross features of the data, but cannot explain some nontrivial details of the measured distributions.

DOI: 10.1103/PhysRevA.70.032501 PACS number(s): 36.10.−k, 34.50.Bw

The energy release by a particle crossing matter is one of the most studied subjects of physics, starting with the seminal paper by Bohr in 1913 [1] and Bethe's theory [2] with its several extensions [3–11]. In Bethe's theory, the energy loss per unit path length (stopping power) is attributed to long-range interactions with the target electrons leading to excitation and/or ionization of the target atoms or molecules. This mechanism will be named electronic stopping power (ESP) in the following. This mechanism is supposed to present an adiabatic lower cutoff, which suppresses its effectiveness at decreasing projectile energies below a few keV. What exactly happens at such energies is not completely known.

On the other hand, at decreasing energy the effect of collisions with the nuclei gives an increasing contribution to the energy loss of a heavy projectile. This mechanism has been called nuclear stopping power (NSP). Several models [12–16] and a few experimental measurements [17–19] exist for $\bar{p}$ NSP.

In the OBELIX experiment [17] the antiproton beam produced at the low-energy antiproton ring LEAR (CERN) was degraded by a suitable thickness of Mylar and entered a target with a continuous energy spectrum from a maximum to zero. Among the other ones, measures were taken with the cylindrical target (useful length=75 cm, diameter =22–30 cm) filled with hydrogen and deuterium at 0.2 mb and helium at 1 and 0.2 mb.

As explained in Refs. [17,18], one of the main peculiarities of our apparatus was the possibility of measuring for each event both the annihilation time (related to the incoming $\bar{p}$ signal) and the vertex coordinates, in particular the depth in the target z. In the following we name scatter plot the set of (z,t) coordinates for annihilation events. This allows for a very detailed analysis of the slowing down and capture features of an antiproton beam in an extended target filled by low-pressure gas, with events distributed in a 75 -cm-long region.

In a previous work [18] by this collaboration ESP for $\bar{p}$ in gaseous hydrogen and helium was reported, for energies as small as 500 eV. Here ESP can be well fitted by the relation $\mathrm{ESP}=\alpha E^{\beta}$, where E is the kinetic energy of the $\bar{p}$. An extrapolation of this relation at lower energies was not sufficient to explain the annihilation scatter plot.

In a further work [19] the scatter plot of $\bar{p}$ at rest annihilations in molecular hydrogen and deuterium gases at 0.2 mb pressure was presented, together with Monte Carlo reproductions of these data. The simulation included ESP as extrapolated from [18] and screened Rutherford $\bar{p}$-nucleus collisions that caused trajectory deflections and beam energy loss in the laboratory frame. To reproduce the scatter plot, a random decay process with lifetimes of 2.1 μs for H_2 and 2.8 μs for D_2 was added after the slowing-down and capture processes. A good reproduction of the data in the whole scatter plot confirmed that below 500 eV the stopping power is dominated by NSP, that this NSP can be reproduced by the simplest available model, and that a large part of the formed exotic atoms are characterized by decay processes with the above lifetimes.

Here we present (z,t) data for annihilation of antiprotons in helium at pressures 1 and 0.2 mb, collected in the same experiment. A Monte Carlo simulation based on the same technique is, in this case, less effective, as discussed below. In fact, despite some features of these data being reasonably similar to the H_2 and D_2 cases, there are some peculiarities that cannot be interpreted as easily as there.

The experimental scatter plot for the collection of (z,t)

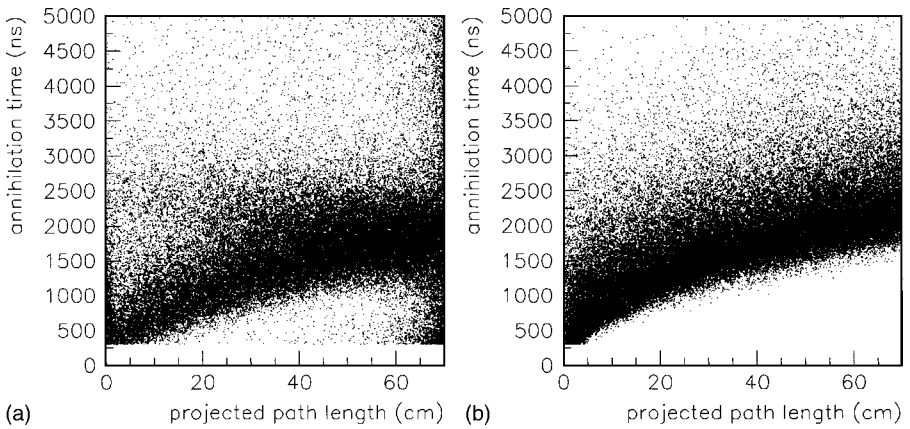

FIG. 1. Experimental (a) and Monte Carlo (b) scatter plot of the $\bar{p}$ annihilation time versus projected path length at 1 mb helium target pressure. Monte Carlo simulations have been performed with many different choices for the parameter values; see Fig. 5 and text. This scatter plot has been simulated with the same parameter values as in Fig. 5(c).

annihilation points is presented in Figs. 1(a) and 2(a) for helium at room temperature and at pressure 1 mb and 0.2 mb, respectively. More detailed time distributions corresponding to 2-cm z slices in the scatter plot are shown in Figs. 3 and 4. Some peculiarities of these figures are general.

The $z \approx 0$ region is characterized by entrance wall annihilations. The data were collected using a temporal gate (above 300 ns and 450 ns, respectively, at 1 mb and 0.2 mb).

For 1-mb data, the vertical belt at large z in the target represents end wall annihilations. In the 0.2-mb case it is not present because in this case the target wessel was longer and the end wall was out of the region covered by the detectors.

Apart from wall effects, most in-gas annihilations are concentrated in a reasonably defined belt which crosses the scatter plot from the origin to the right side. We name it the "main belt" (MB). It includes those antiprotons that have been faster than the other ones in reaching a given z_c capture point and whose cascade process has not been too slow. In each z slice, the MB corresponds to the region surrounding the time distribution peak $t_{peak}(z)$. The $t < t_{peak}$ side of this peak (the "prompt rise") should correspond to those particles that have been the fastest in getting to z_c and whose cascade time has been the shortest. The MB, especially on the prompt rise, is qualitatively similar to the H_2 and/or D_2 cases presented in [19].

Both in the 1-mb and 0.2-mb helium data, the most striking differences with respect to H_2 and D_2 data concern the region of annihilation times $t(z) > t_{peak}(z)$. The fraction of points that are present in this region is much larger in He than in H_2 and D_2. This is especially visible at intermediate times (i.e., not corresponding to long-time cascade tails). In the 1-mb case the intermediate time enhancement is particularly evident, since one can approximately identify a "backward belt" (BB). This BB is visible both in the full scatter plot and in the z slices. It amounts about 10%–20% with respect to the MB (for the meaning of this estimation see below).

The 0.2-mb scatter plot represents a sort of 5-times zooming a small region near the origin of the 1-mb scatter plot. Indeed, both the length of the precapture path and the time needed for post-capture cascade are, roughly speaking, proportional to the helium density. For this reason the BB cannot be fully visible in the 0.2-mb scatter plot (the data taking was limited to 10 μs). Despite this, also in this case a large

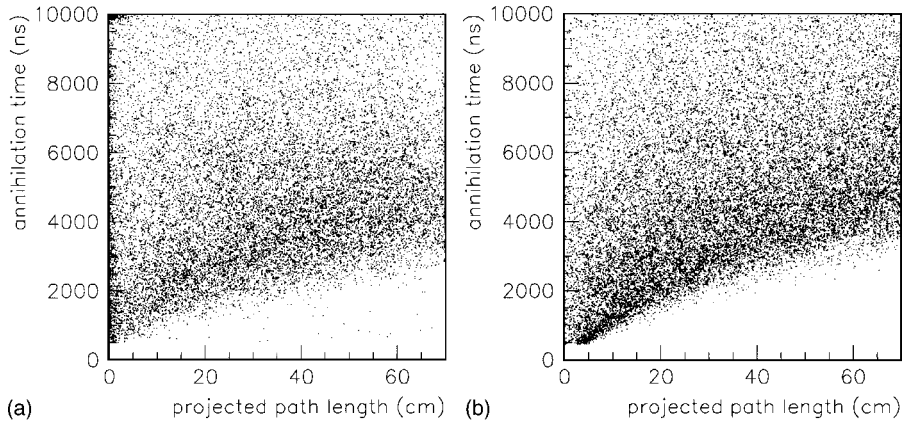

FIG. 2. Experimental (a) and Monte Carlo (b) scatter plot of the $\bar{p}$ annihilation time versus projected path length at 0.2 mb helium target pressure. Monte Carlo simulations have been performed with many different choices for the parameter values; see Fig. 6 and text. This scatter plot has been simulated with the same parameter values as in Fig. 6(c).

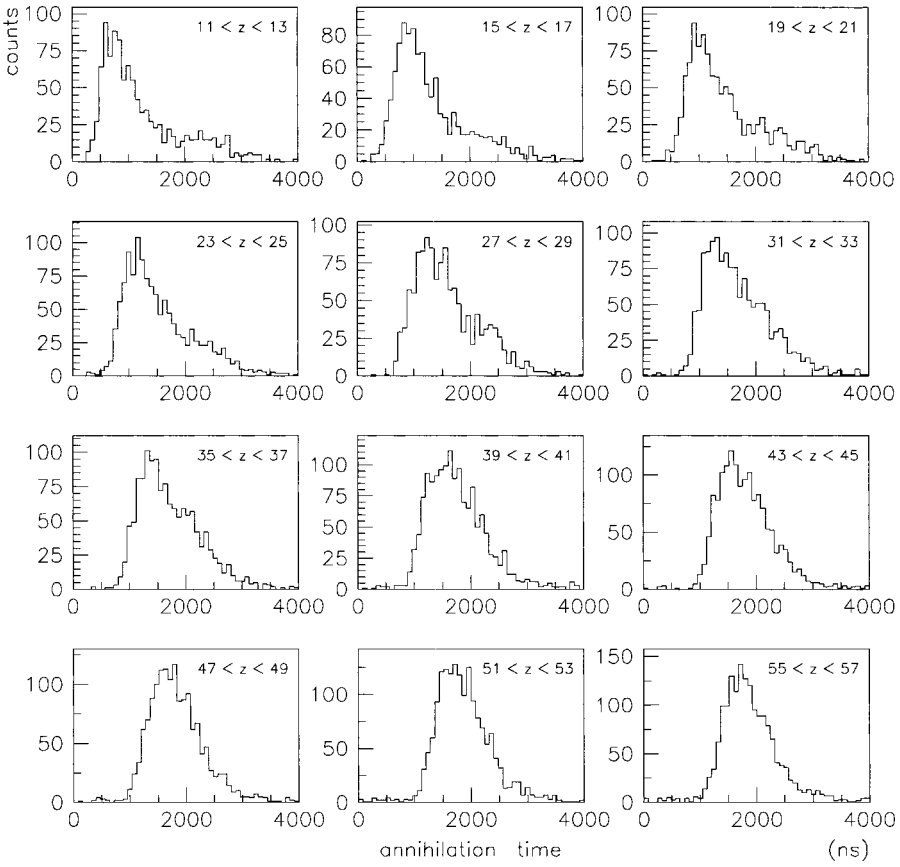

FIG. 3. Experimental annihilation time distribution at different 2-cm zbins in a 1-mb-pressure helium target.

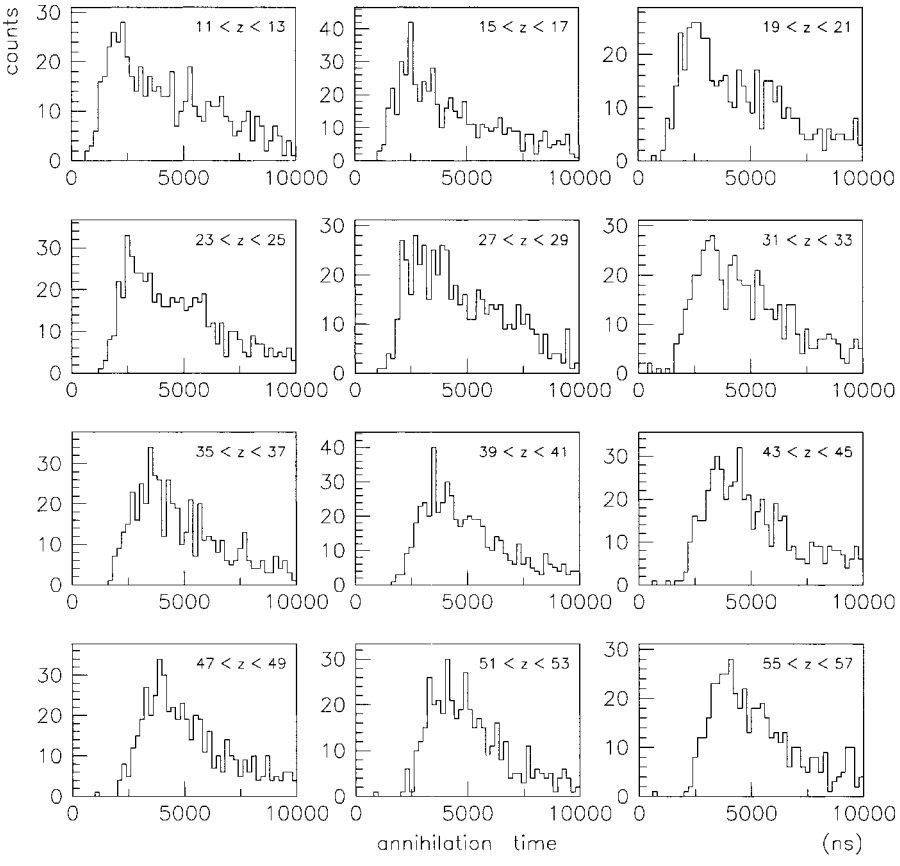

FIG. 4. Experimental annihilation time distribution at different 2-cm *z* bins in a 0.2-mb-pressure helium target.

fraction of annnihilations at intermediate and long times is present. As was done with molecular hydrogen and deuterium, we have tried to fit to each time distribution (for any z slice) a function which is a convolution of a Gaussian and an exponential decay:

$$F(t) = n\int_{-\infty}^{t} \exp\left\{-\frac{(T-t_0)^2}{2\sigma^2}\right\}\exp\left\{-\frac{(t-T)}{\tau}\right\}dT, \quad (1)$$

where n, t_0, σ, and τ are, respectively, the Gaussian normalization factor, mean, width, and exponential lifetime. The underlying idea of this fit is a Gaussian spread due to $\bar{p}$ path fluctuations and an exponential tail because of the cascade. Such a fit is unable to reproduce the time distribution of any of the helium z slices. For each slice we have to decide whether to fit correctly the region of short and intermediate times (which gives too abundant fits at long times) or the region of short and long times (which largely underrates the number of events on the right side of the peak). For the 1 -mb case, a better solution is a fit with a sum of two $F(t)$ functions [Fig. 5(a)]. Despite of the lack of an immediate physical interpretation, one can follow the evolution of this fit through the different z slices and see how the BB is reabsorbed by the MB at increasing z [as evident in Fig. 1(a) too]. In Fig. 6(a), 0.2-mb helium data are fitted by a simple fit of Eq. (1). In Tables I and II we report, for example, typical values of the fit parameters for 1 mb and 0.2 mb helium pressures, respectively, at the different 2-cm z bins of Figs. 5(a) and 6(a). In the 1-mb case the fraction of points reproduced by the second $F(t)$ function is that 10%–20% about which we spoke above.

Before going further, we want to remark that expressions like "long times" do not refer to metastable states in all of the following text. A long cascade time alone is unable to explain the above time distributions, because (i) in each z slice this would reflect in a proportional enhancement at intermediate and at long times, with a steadily positive second derivative of the t distribution at intermediate and long times; (ii) comparing different z slices we should find a roughly z-independent shape of the event decrease on the right side of the peak. Both these features are evident in the Monte Carlo simulations in Figs. 5(b)–5(g), where no fluctuation interrupts the positive trend of the second derivative at intermediate and long times, and the shape of the distribution just t translates compactly for increasing z. But they are contradicted by the data in Fig. 5(a).

The fact that the t distributions change at changing z (apart for the time shift of the prompt rise due to obvious kinematical reasons) can perhaps be related to the dominance of different cascade modes at different z or to multiple scattering. In both cases, however, this leads a z dependence of the shape of the t distributions only in the presence of a different energy spectrum in the $\bar{p}$ beam at different z values.

Starting with constant energy spectrum from zero to several keV at the target entrance, we could imagine that, after some path in helium, a kind of "equilibrium" beam distribution is reached, for $E<1$ keV. In this distribution, the energy distribution is enriched from the higher side by the antiprotons that lose energy in electronic interactions and depleted on the lower side by atomic capture. Also the amount of spread in $\bar{p}$ directions should be connected one to one to the energy, because in Rutherford scattering large-angle deflections are rare at $E \gg 300$ eV. At z large enough for equilibrium to be established, the scatter plot distribution should become z independent, apart from an obvious kinematical displacement towards larger times. This is strikingly evident in the Monte Carlo–simulated scatter plots, which assumed constant energy distributions at the entrance for $E_c<E<6$ keV (see later) (E_c is the capture energy). In the experimental case, we see an equilibrium distribution in the hydrogen case [19]. As shown in Fig. 7 in helium at higher pressures (4, 8.2, 50, and 150 mb, analyzed in [18]) we see evident equilibrium for z larger than few centimeters. As previously remarked when speaking of the density-related "zooming effect" such data correspond to what we could see in the 1-mb case for much larger z than the available ones.

The actual entrance energy distribution is the one determined by degrading materials upstream the target. It has been seen to be regular, with a slow increase, on a keV energy scale [21]; however, the distribution in the $E<100$ eV region is not known with high precision. This energy range is critical because large-angle scattering is most effective here, and the cascade time is supposed to depend on the exact energy at which capture takes place. The clear z dependence of the experimental scatter plots shows that equilibrium, if any, is only reached in the last portion of the target. This makes the analysis of the data complicated, but at the same time it can potentially represent an open window on the energy dependence of $\bar{p}$-helium interactions near the capture region.

Solid Mylar, gaseous molecular hydrogen, and gaseous helium are all different degraders but concerning the capture energy region probably the largest difference is between Mylar and helium, since helium has a much more compact electronic structure than both. So the difference between the target gas equilibrium distribution and the entrance beam composition is probably larger and more effective in the helium target case than in the hydrogen target case, where we see experimentally that equilibrium is fastly reached.

For the Monte Carlo simulation, a collinear beam of 180 000 $\bar{p}$ with constant energy distribution was assumed. To be more precise, the distribution function $f(E)$ for the initial energy of the antiprotons injected into the target is $f(E)=0$ for $E<E_c$ and $E>6$ keV, $f(E)=\text{const}$ for $E_c<E<6$ keV.

Deflections and nuclear stopping power were associated with elastic scattering on a screened Coulomb potential of randomly distributed helium atoms ("screened Rutherford" from now on, with $v=v_{Coulomb}$ for $r<r_{screening}$). Each trajectory was subjected to a continuous energy loss of electronic origin given by the relation $-dE/dx=\alpha E^{\beta}$, with α and β default values taken as the ones suggested by [18]. Actually there is no well-established determination for electronic stopping power at $E<500$ eV, so the use of the above relation at all energies is an extrapolation. As discussed below, also different possibilities were attempted. For a $\bar{p}$-atom distance larger than $r_{screening}$ no direct $\bar{p}$-atom interaction was considered. The phenomenological electronic stopping power αE^{β} includes in itself the effects of long-distance interactions, despite the fact that we are presently unable to relate this

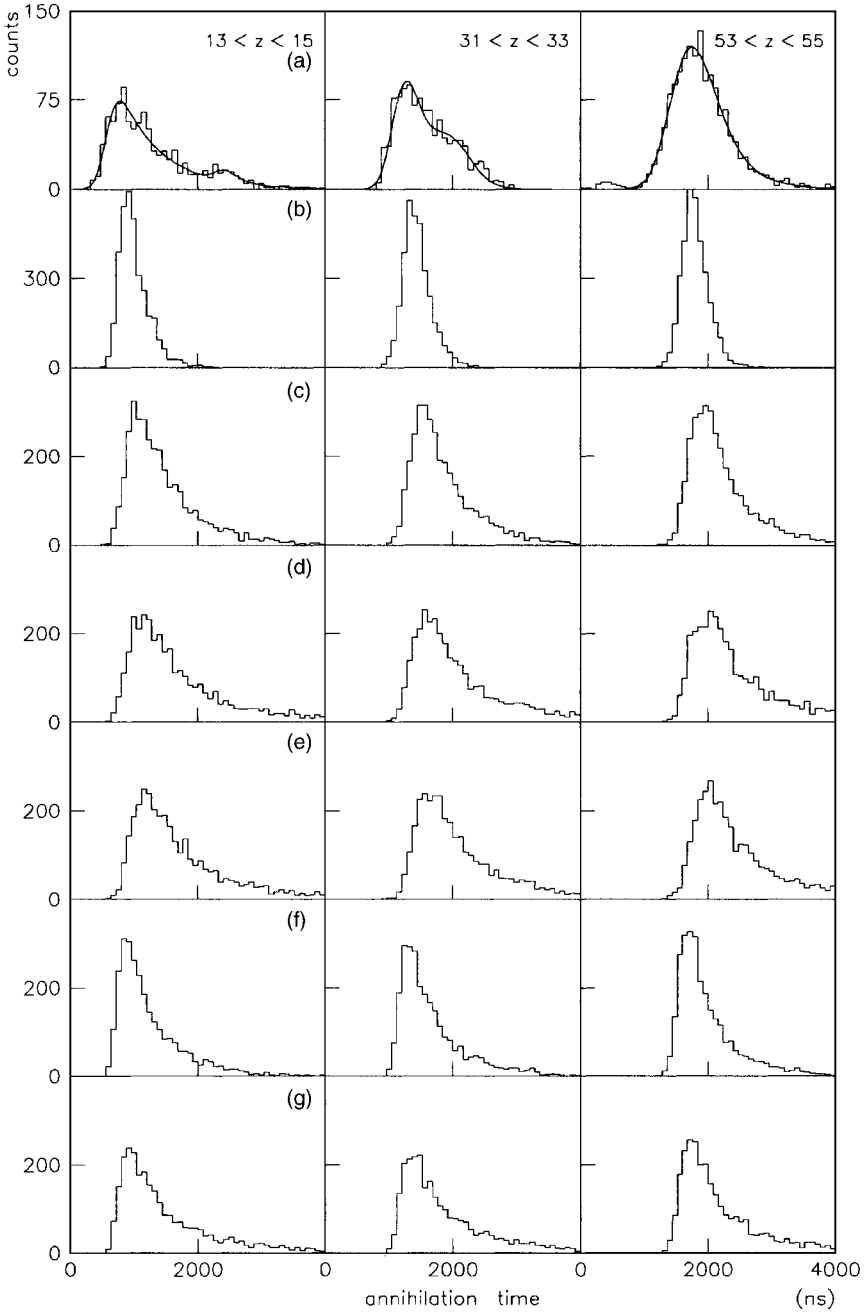

FIG. 5. Experimental (a) and Monte Carlo (b)–(g) annihilation time distribution at different 2-cm z bins in a 1-mb-pressure helium target. (a) Superimposed is the best fitting function (see Table I). (b) Capture energy $E_c=40$ eV, default electronic energy loss [18], no cascade time. (c) Capture energy $E_c=40$ eV, default electronic energy loss [18], two cascade times: 0.1 μs (33%) and 0.6 μs (66%). (d) Capture energy $E_c=40$ eV, default electronic energy loss [18], two cascade times: 0.2 μs (33%) and 1.0 μs (66%). (e) Capture energy $E_c=30$ eV, default electronic energy loss [18], two cascade times: 0.2 μs (33%) and 1.0 μs (66%). (f) Capture energy $E_c=40$ eV, constant electronic energy loss below 600 eV (see text), two cascade times: 0.1 μs (33%) and 0.6 μs (66%). (g) Capture energy $E_c=40$ eV, constant electronic energy loss below 600 eV (see text), two cascade times: 0.2 μs (33%) and 1.0 μs (66%).

assumption to the physics of $\bar{p}$-atom interactions. Capture was assumed as a sudden process taking place at the first $\bar{p}$-atom collision for $\bar{p}$ energy below E_c, with $E_c=10$, 30, 40, 60, 90 eV in different Monte Carlo simulations. For the cascade process we have considered three possibilities: (a) no cascade, (b) an exponential cascade with lifetime with magnitude $1-5$ μs, (c) a two-branch cascade with $1/3$ atoms decaying in a very short time, and $2/3$ atoms decaying as in (b). We did not try to reproduce the regions near the entrance and the end wall of the target, dominated by on-wall annihilations. In Figs. 1(b) and 2(b) we show the Monte Carlo scatter plots for 1-mb and 0.2-mb helium targets, respectively. In Figs. 5(b)–5(g) and 6(b)–6(h) we reported annihilation time distributions producted with different Monte Carlo simulations.

There are of course possibilities to improve this physics

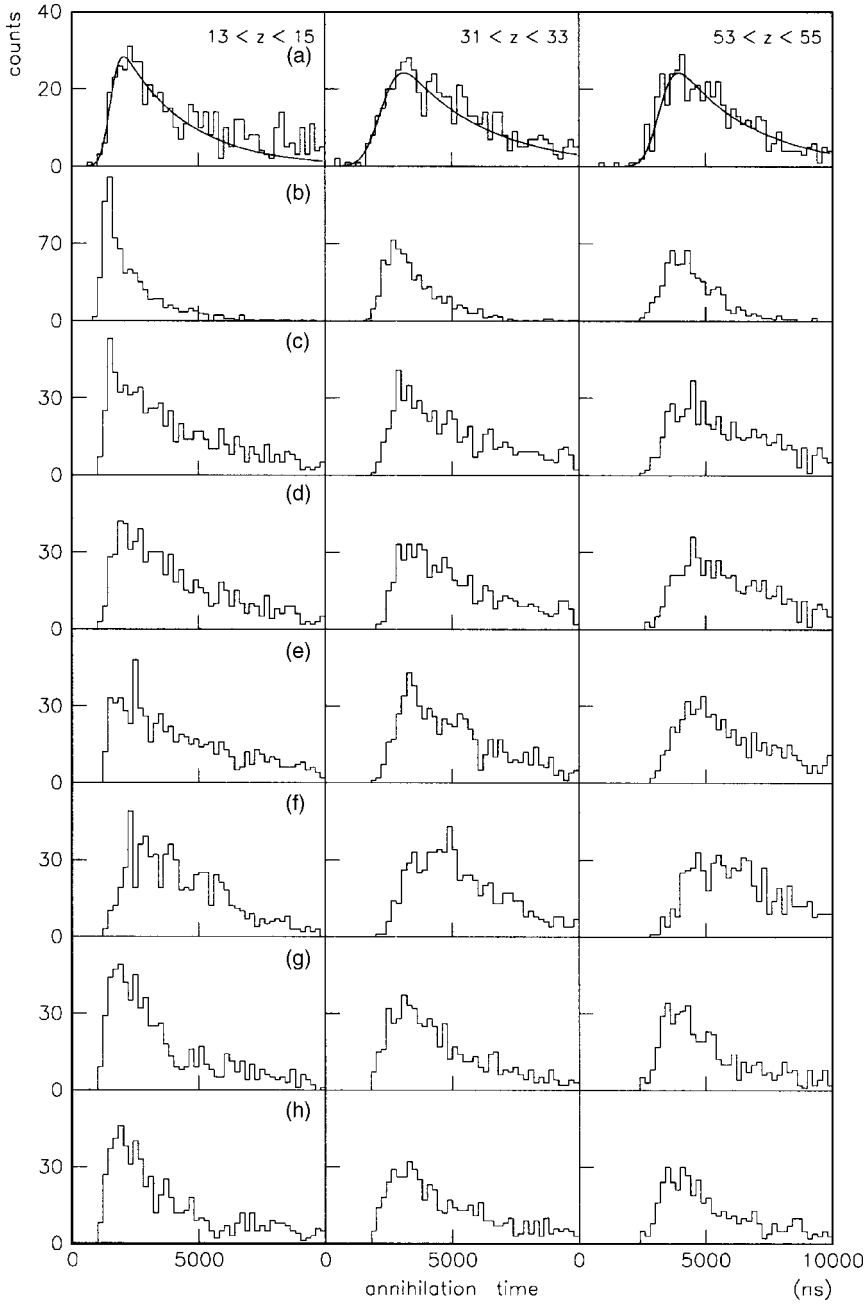

FIG. 6. Experimental (a) and Monte Carlo (b)–(g) annihilation time distribution at different 2-cm z bins in a 0.2-mb-pressure helium target. (a) Superimposed is the best fitting function (see Table II. (b) Capture energy $E_c=40$ eV, default electronic energy loss [18], no cascade time. (c) Capture energy $E_c=40$ eV, default electronic energy loss [18], two cascade times: 0.1 μs (33%) and 3.5 μs (66%). (d) Capture energy $E_c=40$ eV, default electronic energy loss [18], two cascade times: 0.5 μs (33%) and 3.5 μs (66%). (e) Capture energy $E_c=30$ eV, default electronic energy loss [18], two cascade times: 0.1 μs (33%) and 3.5 μs (66%). (f) Capture energy $E_c=30$ eV, default electronic energy loss [18], cascade time 2.0 μs. (g) Capture energy $E_c=40$ eV, constant electronic energy loss below 600 eV (see text), two cascade times: 0.5 μs (33%) and 3.5 μs (66%). (h) Capture energy $E_c=40$ eV, constant electronic energy loss below 600 eV (see text), two cascade times: 0.5 μs (33%) and 5.0 μs (66%).

picture before going to really exotic possibilities. At the level of sophistication employed here some perhaps general conclusions are possible.

(1) As already evidentiated in the hydrogen case [19], a long cascade time τ_c is necessary to reproduce the shape of the data. As shown in Figs. 5(b) and 6(b) where the cascade time is suppressed, the data spread due to screened Rutherford multiple scattering is far smaller than the experimental data spread. E.g., if the above-reported "Gaussian +exponential" fit is applied to $\tau_c=0$ distributions for the 0.2-mb case, it reveals that the multiple-scattering spread produces a large-time tail corresponding to a fictitious $\tau_c \approx 0.5$ μs. An enhancement of the multiple-scattering properties within some model for $\bar{p}$-He interactions may surely af-

TABLE I. Fit parameters to three z-bin different experimental annihilation time distributions of Fig. 5(a), with a sum of two $F(t)$ functions (see text), at a 1-mb helium target. Left, first function fit parameters: n, σ, and t_0 the Gaussian normalization factor, width, and mean value, τ the exponential lifetime; right, second function fit parameters, with the same meaning. The lifetime depends on z, in a way that cannot be justified by fluctuations of the fiting procedure. For this fact we have suggested some explanations (see text), but have no final answer.

z (cm)	n	σ (ns)	t_0 (ns)	τ (ns)	n	σ (ns)	t_0 (ns)	τ (ns)
13–15	72.2	139.1	581.3	657.1	4.3	139.6	2320.0	162.3
31–33	57.6	168.8	1110.0	272.6	26.4	299.8	1904.0	87.6
53–55	99.6	262.6	1477.0	423.8	21.1	358.8	1831.0	102.3

fect intermediate time distributions, but it seems hard to imagine it to produce a fictitious $\tau_c \approx 3-5$ μs. The conclusion is that a conspicuous part of the exotic atoms decays according to a large time behavior $\exp(-t/\tau_c)$ with $\tau_c \approx 0.5-1.5$ μs at pressure 1 mb and $2-5$ μs at pressure 0.2 mb. In the Monte Carlo simulation, the cascade produces a z-independent behavior of large time data in the scatter plot, which does not correspond to our data. For this reason it is difficult to establish a unique value of τ_c.

(2) In each of the simulated z slices, both the post-peak tail and the pre-peak rise are affected by the τ_c choice. As one can see in Figs. 5(c)–5(g) and 6(c)–6(g), adopting τ_c values justified by large-time behavior produces a much softer rise than experimentally observed. On the contrary, the experimental shape of the rise is almost the same as with no cascade. For this reason we conclude that a non-negligible part of the atoms decay with very short average lifetime, and only two-branch cascade Monte Carlo simulations are able to reproduce both the short- and long-time regions. So both a long-τ_c and a short-τ_c component are present in our data. The population of the long-time one seems larger, but magnitudes are similar.

TABLE II. Fit parameters to three z-bin different experimental annihilation time distributions of Fig. 6(a), with a single $F(t)$ function (see text), at a 0.2-mb helium target. The meaning of the parameters is such in Table I.

z (cm)	n	σ (ns)	t_0 (ms)	τ (ns)
13–15	91.8	298.6	1529.0	2523.0
31–33	109.1	565.7	2234.0	3190.0
53–55	98.8	470.6	3211.0	2975.0

(3) Increasing the electronic stopping power leads to two effects: (i) the derivative of line described by the MB in the z-t scatter plot decreases, and (ii)fluctuations (e.g., the time width of the MB peak) decrease. With default values of ESP, the simulated MB derivative is (slightly) larger than observed, but fluctuations are smaller than observed. So any change in the ESP improves one thing but worsens the other one. To understand the effects of an increase of the low-energy ESP, we have first modified the α and β parameters below 600 eV, and as an extreme case we have put constant energy loss for $E<600$ eV. For $E>600$ eV the stopping

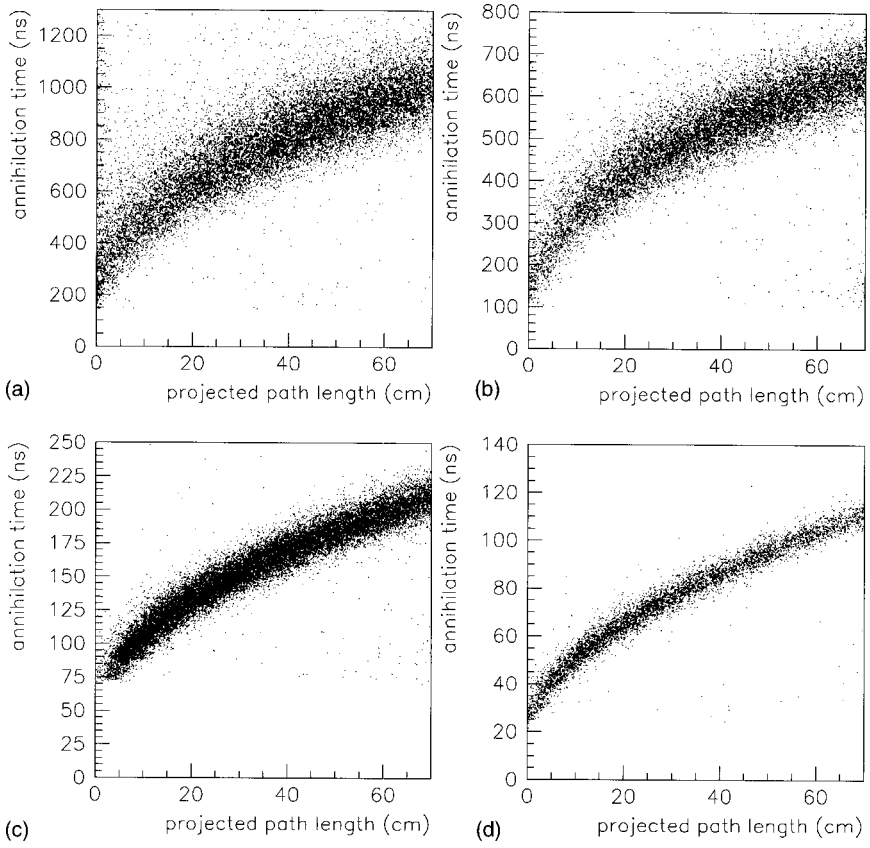

FIG. 7. Experimental scatter plot of the $\bar{p}$ annihilation time versus projected path length at 4 mb (a), 8.2 mb (b), 50 mb (c), and 150 mb (d) helium target pressure [18].

power has been determined elsewhere [18] and we assumed it as fixed. A larger ESP is seen to be more effective in decreasing fluctuations than in decreasing the MB derivative, with the overall effect of leaving default values as the most preferable. The reasons why the effects on the MB position are not large are (i) ESP decreases both z and t for *each* annihilation, but the time-space correlation remains the same, and (ii) when a point is moved away another comes in to substitute it, leaving the MB shape as it is apart from increasing the number of points in the entrance wall region. The fluctuation-depressing effect is caused by the fact that pre-capture fluctuations originate in backscattering events at low energy. If the ESP is small at low energy, the low-energy scattered $\bar{p}$ will complete a long distance with random direction, before capture. As a matter of fact, we do see large fluctuations. The conclusion is that ESP should not be much larger than our default assumption.

(4) The lower edge of the MB contains the fastest particles that have got to a certain z. However, exploration of the Monte Carlo–simulated trajectories of the fastest particles revealed that no antiproton escapes a relevant z decrease related to Rutherford backscattering at energies 50–400 eV. So the prompt rise part of the MB is heavily effected by the properties of the $\bar{p}$-nucleus direct scattering. In addition, differently from ESP, these collisions affect largely the MB position, because of the helium mass. In the limit of an infinite-mass target, nuclear scattering would imply no energy loss, so the same t and a very different z for undeflected and deflected trajectories. So changing the features of the poorly known low-energy $\bar{p}$ atom close collisions would reflect heavily in the shape of the MB, also in the prompt rise zone. The conclusion is that a good reproduction of the short-time side of the MB is a relevant test for models of the low-energy $\bar{p}$-atom collisions.

(5) The capture energy E_c is a critical parameter in reproducing correctly the time distributions at all times [13–16,20]. We recall that the captures in our Monte Carlo simulations happen at the first $\bar{p}$-atom collision with $E<E_c$ in the laboratory frame. We have played with this parameter. Extremes values of it like 10 or 90 eV change too drastically the shape of the distributions. Also 60 eV seems too much, while 30 and 40 eV are almost equally good values, as one can see in Figs. 5 and 6. Within a sharp threshold model for capture, we do not think one can change this parameter too much. On the other hand, we have not attempted nonsharp capture probabilities—i.e., factors of the kind $\exp[(E_c-E)/E_0]$—that would allow for large energy captures without affecting too much the shape of the scatter plot distributions.

(6) The physics assumptions employed for the simulation do not exaust the problem, since a complete reproduction of our data by fine-tuning our parameters was impossible. Common sense suggests that a clear-cut distinction between electron and nuclear stopping power is not justified at low energies. Indeed, electron ionization in the long-range interaction is adiabatically suppressed at $E\sim 100$ eV. Electron ionization is possible in collisions where the $\bar{p}$ penetrates deeply the atomic electron cloud. These are also those processes where $\bar{p}$-nucleus interactions are stronger. A further evolution of the present work could be to simulate the effects of more sophisticated models for the $\bar{p}$-atom interaction, together with a precise reconstruction of the beam energy spectrum at the target entrance. Even if our Monte Carlo reconstruction did reproduce perfectly data, our conclusions should be cautious in front of the possibility of really drastic but correlated changes in some of the several sides of the involved physics assumptions. E.g., a resonance in elastic scattering at energy $\sim$100 eV would lead to a much larger amount of time fluctuations, which would permit us to increase the low-energy ESP and/or to decrease the cascade lifetime. Or a complete disappearance of ESP below 100 eV would enhance the effects of multiple scattering on large-time fluctuations, which presently we explain almost completely in terms of cascade time.

(7) As an example of explanation of the backward belt, let us assume the capture energy as distributed on a wide energy range, so that at $E<40$ eV all $\bar{p}$ are captured, but capture is possible also at much larger energies—say, at $E\approx 70$ eV. This may occur if double ionization of the target atom takes place in a collision and seems a more realistic model than the sharp capture threshold used here. This capture energy spread has two consequences: (i) a wide (N,L) distribution of the initial states of the exotic atom and ion A and (ii) a wide distribution of the recoil velocities v_r of A. We cannot say easily about the consequences of point (i), but concerning point (ii) we know that the average cascade time of a nonmetastable A is approximately proportional to the number of A-atom collisions. So we have roughly $\tau_c \propto 1/v_r \propto 1/\sqrt{E_c}$. This phenomenon is enhanced if the $\bar{p}$ energy distribution at the entrance is populated by antiprotons with $E \ll 40$ eV. We expect this to happen in the first part of the target. In the second part of the target the high helium capture cross section for $E<40$ eV will not allow many such antiprotons to survive. The consequence would be a particularly wide distribution of cascade times as far as all $\bar{p}$ with $E<30$ eV have not disappeared. If, on the contrary, the explanation of the BB had to be searched in the high-energy capture events, a detail that should be taken into account is the entrance energy of the $\bar{p}$ involved in the BB. This energy ranges from zero to about 3 keV. Rare fluctuations apart, a larger entrance energy leads to $\bar{p}$ capture at z values where the BB has been reabsorbed by the main belt. More difficult is to explain the BB in terms of trajectory spread, because one would expect this phenomenon to be more effective at increasing z, oppositely to what is seen. In a not too evident form, this effect can be seen in the higher-pressure helium data and in hydrogen data. However, a backward belt associated with relevant straggling phenomena at small z would be possible, for example, if rare capture, no ESP, and only very small impact parameter collisions were present at $E<40$ eV (see, e.g., [9]). This would imply large deflections accompanied by a long time delay before capture.

To summarize, we have presented the z, t scatter plots of $\bar{p}$-helium low-energy annihilations for helium pressure at 0.2 and 1 mb. We have also presented the corresponding time distributions for 2-cm z slices. Both the scatter plots and the time distributions show relevant qualitative differences with respect to the corresponding data in molecular hydrogen and deuterium. Annihilation points are more abundant than ex-

pected at intermediate times, where it is impossible for us to distinguish between post-capture cascade effects and pre-capture multiscattering effects. A previous Monte Carlo technique, successful in reproducing H_2, D_2 data, was employed here, with much smaller effectiveness. A discussion of the effects of tuning the simulation parameters has been presented, with qualitative conclusions concerning the effects of the different physical ingredients.

[1] N. Bohr, Philos. Mag. **25**, 10 (1913).
[2] H. A. Bethe, Ann. Phys. (Leipzig) **5**, 325 (1930).
[3] E. Fermi and E. Teller, Phys. Rev. **72**, 399 (1947).
[4] F. Bloch, Ann. Phys. (Leipzig) **16**, 287 (1933).
[5] W. H. Barkas, J. N. Dyer, and H. H. Heckman, Phys. Rev. Lett. **11**, 26 (1963).
[6] M. Inokuti, Rev. Mod. Phys. **43**, 297 (1971).
[7] J. F. Ziegler, J. P. Biersack, and U. Littmark, *The Stopping and Range of Ions in Solids* (Pergamon, Oxford, 1985).
[8] H. Knudsen and J. F. Reading, Phys. Rep. **212**, 107 (1992).
[9] G. Schiwietz, U. Wille, R. Diez Muino, P. D. Fainstein, and P. L. Grande, J. Phys. B **29**, 307 (1996).
[10] T. B. Quinteros and J. F. Reading, Nucl. Instrum. Methods Phys. Res. B **53**, 363 (1991).
[11] P. Sigmund and A. Schinner, Eur. Phys. J. D **15**, 165 (2001).
[12] S. A. Wightman, Phys. Rev. **77**, 521 (1950).
[13] W. A. Beck, L. Wilets, and M. A. Alberg, Phys. Rev. A **48**, 2779 (1993).
[14] J. S. Cohen, Phys. Rev. A **62**, 022512 (2000).
[15] G. Ya. Korenman, Nucl. Phys. A **692**, 145c (2001).
[16] J. S. Briggs, P. T. Greenland, and E. A. Solov'ev, Hyperfine Interact. **119**, 235 (1999).
[17] A. Adamo *et al.*, Phys. Rev. A **47**, 4517 (1993).
[18] M. Agnello *et al.*, Phys. Rev. Lett. **74**, 371 (1995).
[19] A. Bertin *et al.*, Phys. Rev. A **54**, 5441 (1996).
[20] A. Y. Voronin and J. Carbonell, Hyperfine Interact. **115**, 143 (1998).
[21] M. Corradini *et al.*, (unpublished).